AGU PUBLICATIONS

Geophysical Research Letters

RESEARCH LETTER
10.1002/2014GL060450

Key Points:
- Emission of MHD waves from the BBF channel boundaries due to KHI is possible
- Observed BBFs and MHD waves association can be explained by KHI generated waves
- KHI waves may extract energy from BBF and cause flow braking

Correspondence to:
H. Turkakin,
turkakin@ualberta.ca

Citation:
Turkakin, H., I. R. Mann, and R. Rankin (2014), Kelvin-Helmholtz unstable magnetotail flow channels: Deceleration and radiation of MHD waves, *Geophys. Res. Lett.*, *41*, 3691–3697, doi:10.1002/2014GL060450.

Received 8 MAY 2014
Accepted 13 MAY 2014
Accepted article online 17 MAY 2014
Published online 2 JUN 2014

Kelvin-Helmholtz unstable magnetotail flow channels: Deceleration and radiation of MHD waves

H. Turkakin[1], I. R. Mann[1], and R. Rankin[1]

[1]Department of Physics, University of Alberta, Edmonton, Alberta, Canada

Abstract The Kelvin-Helmholtz instability (KHI) of magnetotail flow channels associated with bursty bulk flows (BBFs) is investigated. MHD oscillations of the channel in both kink and sausage modes are investigated for KHI, and both the primary and secondary KHIs are found that drive MHD waves. These instabilities are likely to be important for flow channel braking where the KHI removes energy from the flow. At flow speeds above the peak growth rate, the MHD modes excited by KHI develop from surface modes into propagating modes leading to the radiation of MHD waves from the flow channel. The coupling of BBF-driven shear flow instabilities to MHD waves presented here represents a new paradigm to explain BBF excitation of tail flapping. Our model can also explain, for the first time, the generation mechanism for the observations of waves propagating toward both flanks and emitted from BBF channels in the magnetotail.

1. Introduction

Earthward bursty bulk flows (BBFs) with flow speeds varying between 200 and 1500 km/s have been observed in the central plasma sheet for decades [e.g., *Baumjohann et al.*, 1990; *Angelopoulos et al.*, 1992, 1997; *Shiokawa et al.*, 1997]. These BBFs start at distances $x_{GSM} \lesssim -20\ R_E$ and are stopped at distances about $x_{GSM} \simeq -6\ R_E$ [e.g., *McPherron et al.*, 2011]. The details of the braking mechanism of these earthward BBFs remains unclear with deceleration due to magnetic field dipolarization [e.g., *Shiokawa et al.*, 1997] or due to Kelvin-Helmholtz instabilities [e.g., *Volwerk et al.*, 2007] both having been postulated. Both kink- and sausage-type oscillations of the current sheet, propagating either along the magnetotail or toward the tail flanks, are also often observed, these flankward waves having been suggested as being driven by a poorly understood emission process in the central part of the magnetotail [e.g., *Sergeev et al.*, 2004]. Observations have suggested that such oscillations may be initiated by earthward BBFs in the central plasma sheet [e.g., *Volwerk et al.*, 2005] and the boundaries of the BBFs may possibly be Kelvin-Helmholtz unstable [e.g., *Volwerk et al.*, 2007]. However, theoretical details of the relationship between the wave excitation, especially those propagating toward both flanks, and the BBFs has not been established.

In this paper we investigate the excitation of MHD waves by the Kelvin-Helmholtz instability (KHI) on flow channels in the plasma sheet, such as earthward BBFs, following the suggestion by *Volwerk et al.* [2007, 2008]. Our results show that both slow and fast kink and sausage MHD waves may become KH unstable at sufficiently fast flow speeds, resulting in the primary and secondary KHIs, respectively [cf. *Turkakin et al.*, 2013]. We further investigate the possibility that the KHI may cause the emission of MHD waves from the shear flow boundary in a similar manner to that suggested by *Mann et al.* [1999] as applied to the magnetopause. Our results are significant as the first numerical results showing not only that the KHI is a plausible physical mechanism for braking BBFs but also that the emission of MHD waves from the flow channels can be triggered by KHI process. Our results can provide for the first time an explanation for the observations of flankward propagating waves, sometimes described as tail flapping, which can be emitted from such flow channels in the magnetotail [cf. *Sergeev et al.*, 2004; *Volwerk et al.*, 2005]. Two earlier models of magnetic double gradient and ballooning instability waves in a curved magnetic field were suggested by *Erkaev et al.* [2008] and *Golovchanskaya and Maltsev* [2005] to explain tail flapping modes. However, as described by *Forsyth et al.* [2009]: *"Neither of the models considers the generation mechanism for the flapping motion of the plasma sheet, only the mechanism that supports the wave propagation."* Our paper provides the first theoretical framework which explains the link between BBFs, KHI, and the excitation of wave modes such as tail flapping by tail flows. It is also the first to consider MHD wave emission from the flow channel toward the flanks, excited by shear flow KH instability.

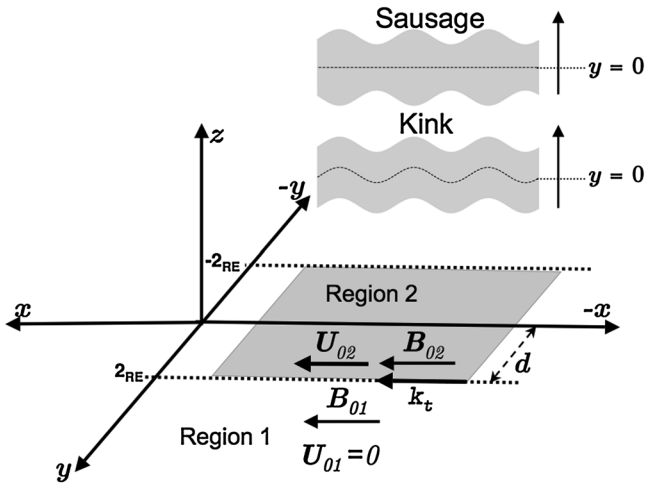

Figure 1. Coordinate system considered for calculations of BBF initiated KHI waves. Chosen to be analogous to GSM are x, y, z coordinate directions. Region 1 is out of the channel, and region 2 is inside the channel. Boundary of the flow channel lies at $y = \pm d = \pm 2\ R_E$.

2. Flow Channel Model Geometry and Boundary Conditions

A simplified 1-D flow channel model is used consisting of a plasma sheet flow channel separated by a thin boundary from a semi-infinite plasma sheet. Since the magnetic field orientation is mainly along x_{GSM} in the magnetotail, this model provides a good approximation to the tail [c.f. *Sergeev et al.*, 2004]. A box model whose coordinates are analogous to GSM (geocentric solar magnetic) coordinate system is used. The y coordinate has flow channel boundaries at $y = \pm d$ as illustrated in Figure 1. Region 1 represents the external magnetotail plasma sheet, and region 2 represents the flow channel. The background magnetic fields in regions 1 and 2, $B_{01,02}$, are set parallel to the flow channel boundary, and the background flow velocity, U_{01}, is set to zero and $U_{02} > 0$ directed along positive x. Since the wave behavior of kink and sausage waves analyzed here is symmetric about $y = 0$, we have considered a domain assumed to be half of the flow channel for $y > 0$. We adopt a symmetric inner boundary in the midchannel and half-channel width of d. A tangential discontinuity (TD) with zero transition thickness is assumed at $y = d$ which is a valid model for long-period KHI waves with wavelengths much larger than the thickness of the transition layer.

3. MHD Wave Model

We follow the standard approach where the ideal MHD equations are linearized under a small-amplitude approximation for compressible warm homogeneous plasmas on both sides of the flow channel boundary. We have assumed space and time variation of the form $\simeq De^{i(\mathbf{k}.\mathbf{r}-\omega t)}$, where ω is the complex frequency, $\mathbf{k}$ is the wave number, and D is a constant.

We consider two types of MHD wave modes, kink and sausage surface waves, that are observed along the plasma sheet flow channel boundaries [e.g., *Sergeev et al.*, 2003; *Volwerk et al.*, 2005]. The sausage modes are characterized by expansion and contraction, and the kink modes are characterized by wavy flapping motion of the flow channel [cf., *Roberts*, 1991]. The general oscillation characteristics of the kink and sausage modes are illustrated in the top right corner of Figure 1.

MHD wave solutions in regions 1 and 2 are connected through TD boundary conditions, namely, continuity of normal displacement, δy, and total pressure perturbations, δp_t, across the flow channel boundary. Therefore, matching conditions across the boundary between regions 1 and 2 are $\delta p_{t1} = \delta p_{t2}$ and $\delta y_1 = \delta y_2$. The inner boundary conditions in the midchannel, $y = 0$, are different for the kink and sausage modes, since the kink modes will have an antinode and sausage modes will have a node at this position. Hence, the boundary condition at $y = 0$ for the kink modes is $\frac{d\delta v_{y2}}{dy} = 0$, from which it follows that $\delta p_{t2} = 0$, and those of sausage modes are $\delta v_{y2} = 0$, and $\frac{d\delta p_{t2}}{dy} = 0$, where δv_{y2} is the perpendicular velocity perturbation

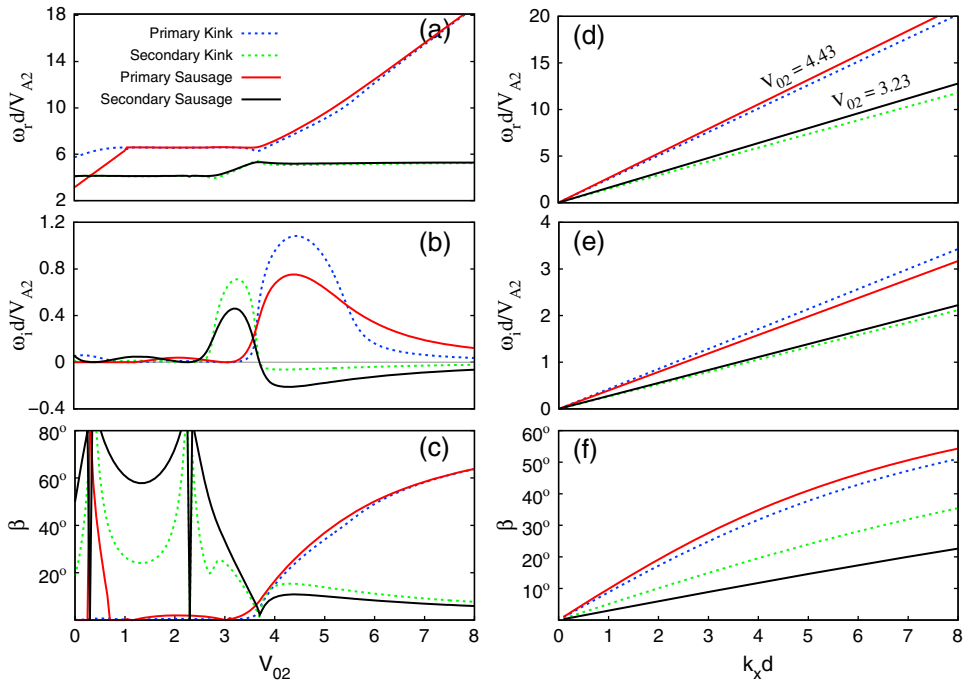

Figure 2. The variations of real and imaginary frequencies and the propagation angle as a function (a–c) of the background flow speed, $V_{02} = U_{02}/V_{A2}$, and (d–f) of the normalized tangential wave number, $k_x d$.

in the flow channel, region 2. With the above boundary conditions MHD kink modes are governed by the equation

$$i\cot(k_{y2}d)\left[\left(\omega_1'\right)^2 - \left(\mathbf{V}_{A1}\cdot\mathbf{k}_t\right)^2\right]\frac{\rho_{01}}{k_{y1}} + \left[\left(\omega_2'\right)^2 - \left(\mathbf{V}_{A2}\cdot\mathbf{k}_t\right)^2\right]\frac{\rho_{02}}{k_{y2}} = 0, \tag{1}$$

and MHD sausage modes are governed by the equation

$$i\tan(k_{y2}d)\left[\left(\omega_1'\right)^2 - \left(\mathbf{V}_{A1}\cdot\mathbf{k}_t\right)^2\right]\frac{\rho_{01}}{k_{y1}} - \left[\left(\omega_2'\right)^2 - \left(\mathbf{V}_{A2}\cdot\mathbf{k}_t\right)^2\right]\frac{\rho_{02}}{k_{y2}} = 0, \tag{2}$$

where $\omega'_{1,2} = \omega - \mathbf{U}_{01,02}\cdot\mathbf{k}_t$ are the Doppler-shifted frequencies, $\mathbf{V}_{A1,A2}$ are the Alfvén speeds, and $k_{y1,y2}$ are wave numbers normal to the boundary, in regions 1 and 2, respectively.

The eigenfrequencies of equations (1) and (2), representing kink and sausage wave modes, respectively, are computed numerically using a Newton-Raphson scheme, yielding complex eigenfrequencies for a set of given parameters. In the following sections of the paper normalized flow velocities $V_{01,02}$ are used such that $V_{01,02} = U_{01,02}/V_{A2}$ with normalization with respect to the Alfvén speed, V_{A2}, in the flow channel, region 2. The distance, d, is normalized by R_E, and wave numbers, k_x, k_y, are normalized by $1/d$. Normalized frequencies are real frequencies, $\omega_r d/V_{A2}$, and growth rates, $\omega_i d/V_{A2}$. Assuming hydrogen plasma, the background physical parameters are set such that densities $\rho_{01}/\rho_{02} = 0.75$, $B_{01}/B_{02} = 1.8$, $V_{A1}/V_{A2} = 2.1$, $\beta_1 = 0.78$, and $\beta_1 = 4.88$ which are observable values in the plasma sheet regions [e.g., *Angelopoulos et al.*, 1992; *Volwerk et al.*, 2007, 2008]. The adiabatic index γ is taken as 5/3, and $d = 2\,R_E$ which is an appropriate value for flow channel half thickness [c.f., *Nakamura et al.*, 2004]. A normalized tangential wave number is chosen such that one wavelength would fit in the half flow channel, $k_t = 2\pi/d$, and directed along $+x$, $k_t = k_x$, and waves propagate in the plane of the tail such that $k_z = 0$ (see Figure 1).

4. Results

The eigenfrequency variation with increasing normalized flow speed, $V_{02} = U_{02}/V_{A2}$, in the channel is shown in Figures 2a and 2b, where both kink and sausage modes show two distinct K-H unstable regions representing primary and secondary KHIs [c.f., *Turkakin et al.*, 2013]. The secondary KHI becomes unstable at lower BBF flows, $V_{02} \simeq 2.8$, than primary KHI, $V_{02} \simeq 3.3$, which agrees with the results in *Turkakin et al.* [2013]. Figures 2a and 2b show that the primary and secondary sausage modes (red and black solid lines) have slightly larger

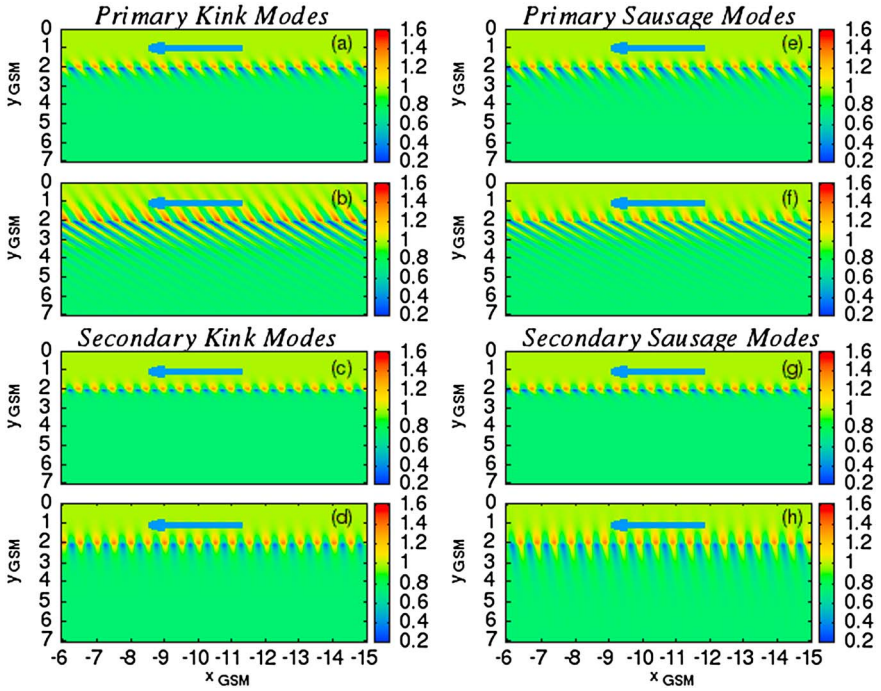

Figure 3. Normalized plasma density profiles of the eigenmodes of the primary and secondary (a–d) kink and (e–h) sausage KHI waves on the flow channel boundary. Figures 3a and 3e show the primary kink and sausage KHI waves at their peak growth rate, $V_{02} = 4.45$ and $V_{02} = 4.4$, respectively. Figures 3b and 3f during MHD wave emission at $V_{02} = 5.5$. Similarly, Figures 3c and 3g show the secondary kink and sausage modes at their peak growth rate, $V_{02} = 3.25$ and $V_{02} = 3.2$, respectively, and Figures 3d and 3h during period of MHD wave emission for $V_{02} = 3.65$. Emission of MHD waves from the shear flow boundary is visible for $V_{02} \gtrsim 5.5$ for primary KHI and for $V_{02} \gtrsim 3.65$ for secondary KHI.

real frequencies and smaller growth rates than the kink modes (blue and green dashed lines). Since the primary KHI onsets occur at larger background flow speeds, V_{02}, it is possible that both primary and secondary KHIs may be important during BBF evolution. For example, primary KHI excited kink and sausage modes could be generated during the bursts within the BBFs which can have flow speeds reaching up to 1500 km/s and which last for about 2–4 min [c.f., *Angelopoulos et al.*, 1997; *Shiokawa et al.*, 1997]. Secondary KHI kink and sausage modes might be excited more continuously during the core of BBFs where the flow speed can reach up to 700 km/s and last about 10–30 min [e.g., *Angelopoulos et al.*, 1992; *Nakamura et al.*, 2004], or at slower speeds during BBF deceleration.

We also calculated the phase velocities, $\mathbf{U_p} = \frac{\omega_r}{(k_x^2+k_y^2)}\mathbf{k}$, periods, $T_r = 2\pi/\omega_r$, and the propagation angles with respect the background flow, $\beta = \tan^{-1}(k_y/k_x)$ for these modes. Normalized phase velocities show that the primary kink and sausage modes are fast waves, while the secondary kink and sausage modes are slow waves in the stationary plasma frame in region 1 (not shown here) consistent with the results shown in *Turkakin et al.* [2013]. Variations of propagation angles, β, with background flow are displayed in Figure 2c and are found to vary between $\simeq 0°$–$64°$ for primary and $\simeq 0°$–$40°$ for secondary KHI waves. Sharp peaks in the propagation angles of the secondary KHI waves happen at flow speeds below that for the onset of instability and are the result of a slow resonance [c.f., *Kozlov and Leonovich*, 2011], analysis of which is beyond the scope of this paper. With the use of an appropriate Alfvén speed in the channel as 200 km/s, we have calculated the periods and wavelengths of the MHD waves emitted from the BBF boundary. The periods vary between $\simeq 10$ and 70 s and wavelengths vary between $\simeq 2$ and 4 R_E for both growing primary and secondary KHI waves. These values are in good agreement with the observed values of the waves along the plasma flow channels [e.g., *Sergeev et al.*, 2003; *Volwerk et al.*, 2004, 2008]. We also investigated the effects of the magnetic tilt along the z_{GSM} direction in the flow channel and found that the growth rates increase with the increasing magnetic tilt (not shown).

We also explored the dependence of the eigenmodes on the normalized tangential wave number, $k_x d$, at a specific BBF speed, selecting $V_{02} = U_{02}/V_{A2} = 4.43$ for primary KHI waves and $V_{02} = U_{02}/V_{A2} = 3.23$ for

secondary KHI waves where both kink and sausage modes growth rates are close to maximum (see Figure 2b). The results are shown in Figures 2d–2f. As expected for a zero thickness boundary, the normalized real frequencies and growth rates of both kink and sausage primary and secondary KHI waves monotonically increase with $k_x d$ [e.g., *Mann et al.*, 1999] (see Figures 2d and 2e). As $k_x d$ increases, the primary and secondary KHI kink modes propagation direction approach 51° and ≃35°, respectively, while that of the sausage modes approach ≃54° and ≃23°, respectively. This result is in very good agreement with the observed values for the propagation directions of the waves seen in association with BBFs, varying between ≃30°–48° with respect to the flow boundary [e.g., *Sergeev et al.*, 2003; *Volwerk et al.*, 2004, 2008].

Density profiles of the kink and sausage modes reveal that wave propagation away from the flow channel is possible during the KHI process. Figure 3 shows eigenmode density profiles for the primary and secondary KHI kink modes (Figures 3a–3d) and sausage modes (Figures 3e–3g). Figures 3a and 3e display the density profiles of the primary KHI modes at the peak growth rates, flow speed $V_{02} = 4.45$ for the primary kink mode (Figure 3a) and $V_{02} = 4.4$ for the primary sausage mode (Figures 3e). Figures 3b and 3f show the profiles at $V_{02} = 5.5$. It is clearly visible in Figures 3b and 3f that both the kink and sausage primary KHI modes excite waves which propagate away from the flow channel at $V_{02} = 5.5$. The secondary kink and sausage mode density profiles are also shown at background flow speeds values at peak growth rates, $V_{02} = 3.25$ for the secondary kink modes (Figure 3c) and $V_{02} = 3.2$ for the secondary sausage modes (Figure 3g), as well as at a larger flow speed, $V_{02} = 3.65$ (Figures 3d and 3h). The secondary KHI modes are also able to excite waves which propagate out of the flow channel boundary after a certain value of the flow speed is reached. There is a considerable difference, however, between the flow speed at which the transition from predominantly surface to a propagating mode takes place: $V_{02} = 5.5$ for the primary and $V_{02} = 3.65$ for the secondary KHI. Observations have shown that these normalized flow speed values can be reached during a BBF in the central plasma sheet [c.f. *Angelopoulos et al.*, 1992] (Figure 4 c).

These results illustrate cases of the emission of magnetosonic waves from the boundary of a moving medium [*Landau and Lifshitz*, 1987; *Mann et al.*, 1999] which in the current study are applied to the BBF channel dynamics in the magnetotail and which offer an explanation for the waves observed to be emitted from BBF channels in the central plasma sheet. Our results also suggest that the energy in the BBFs may be fed into primary and secondary KHI kink and sausage modes, including into waves emitted from the flow channels, causing BBF braking in the near-Earth region.

Figure 4 displays the spatial variation of the eigenmode profiles across the flow channel boundary at $V_{02} = 5.5$ for the primary KHI modes, and $V_{02} = 3.65$ for the secondary KHI modes where emission of MHD waves from the BBF channel is present (c.f. Figures 3b, 3f, 3d, and 3h). What is very clear in Figure 4 is that the amplitude of the perturbed velocity and magnetic fields peaks at the shear flow boundary at the edge of the BBF, as expected. Also clear in Figure 4 is that there is considerable oscillating eigen-structure as a function of y at constant x for the primary KHI and not for the secondary KHI, despite propagating MHD waves being emitted from the boundary in both cases. The explanation, of course, relates to the angle of propagation of the phase fronts of the propagating modes outside the BBF in each case. Overall, both the primary and secondary KHI kink and sausage modes may be able to extract kinetic energy from the background flow and impact the flow evolution and braking of BBFs as they travel toward the Earth.

We have calculated mode group speeds using the eigenfrequencies and wave numbers obtained above using the equation $U_{gr} = \frac{d\omega}{dk}$. We also calculated the e-folding growth times and distances traveled by wave packets using the group speeds during an e-folding time, i.e., e-folding length, in search of energy dissipation efficiency by the primary and secondary KHI kink and sausage waves. We have again assumed a value of the physical Alfvén speed in the region 2 as 200 km/s and calculated the physical values of e-folding times and e-folding lengths using this Alfvén speed. At the flow speed values for peak growth rates, the primary kink and sausage modes e-folding times are calculated as 58.8 and 84.6 s, respectively. Their normalized group speeds, $V_{gr} = U_{gr}/V_{A2}$, i.e., the speed of energy propagation, along the flow are calculated to be 1.84 for the primary kink and 1.82 for the primary sausage waves. With these group speeds the e-folding lengths of the primary kink and sausage wave are calculated to be $\simeq 3.4\,R_E$ and $\simeq 4.8\,R_E$, respectively. Therefore, these waves will travel distances ≃7–10 R_E during two e-folding times which is an appropriate distance compared to that which the BBFs generally travel from the tail to the near-Earth region during flow braking. This shows that the primary kink and sausage KHI waves may grow sufficiently fast to be able to dissipate a significant amount of the initially available kinetic energy of the flow causing flow braking in the near-Earth

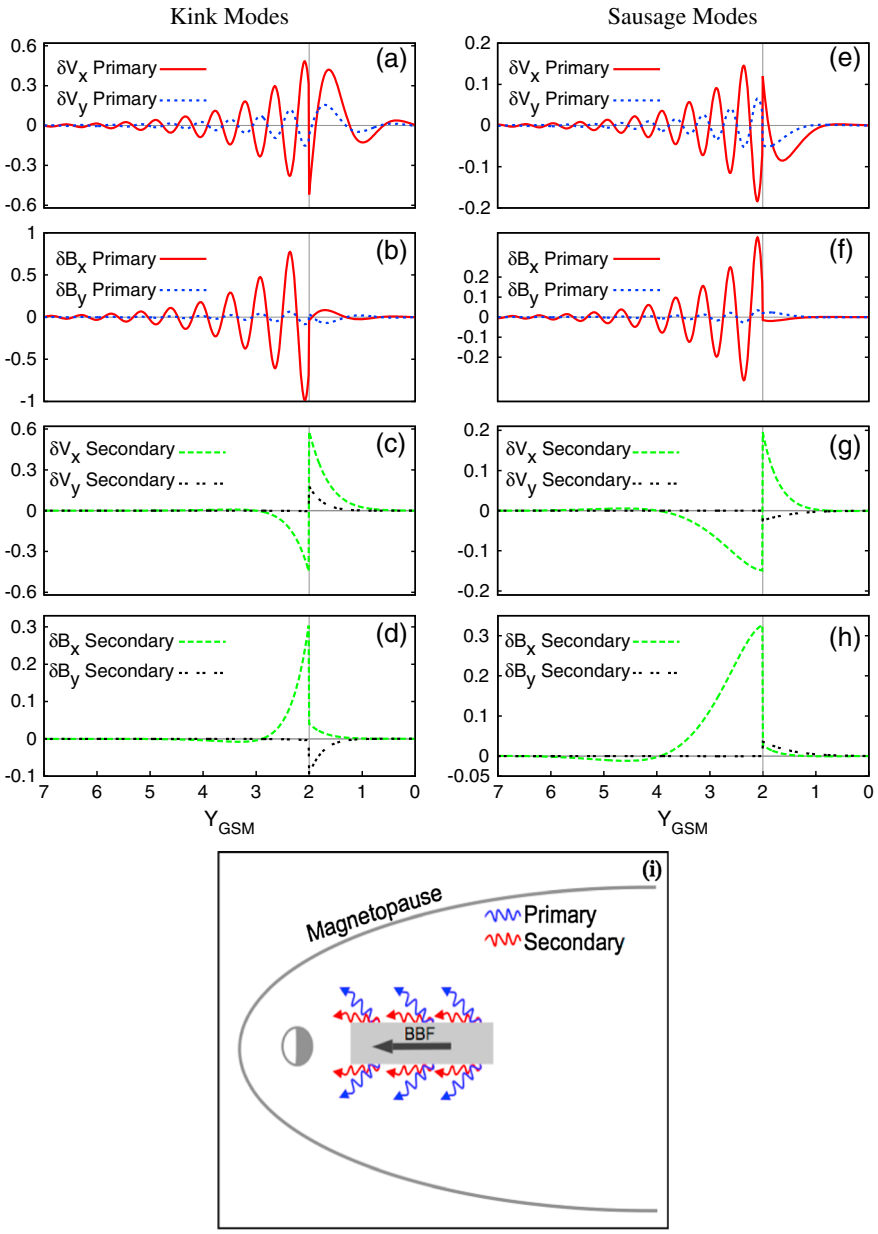

Figure 4. The eigenmode profiles of perturbed *x* and *y* components of normalized magnetic field and velocity variation across the flow channel boundary for primary and secondary (a–d) kink and (e–h) sausage modes. $V_{02} = 5.5$ for the primary modes and $V_{02} = 3.65$ for the secondary modes, with the same parameters as in Figures 3b and 3f for the primary, in Figures 3d and 3h for the secondary KHI modes. (i) The schematic showing the characteristics of the propagation direction of kink and sausage modes which are excited by the KHI at the edges of the BBF channel.

region. The secondary KHI kink and sausage modes are found to have group speeds along the flow as 1.85 and 1.74 at the growth rate peaks and *e*-folding times of $\simeq 89.5$ and $\simeq 138.4$ s resulting *e*-folding lengths of $\simeq 4.7\,R_E$ and $\simeq 7.5\,R_E$, respectively. Therefore, these waves will travel distances $\simeq 10$–$16\,R_E$ during two *e*-folding times which could also be appropriate for BBF flow braking. Although not as fast growing as the primary modes, these secondary modes may also grow fast enough to cause flow braking. These results also display the fact that the primary and secondary KHI kink modes can dissipate energy somewhat faster than those of the sausage modes. Since the growth rates increase with increasing angle between the flow and the background magnetic field (not shown), it is possible that as the waves move closer to the Earth, the increase of the magnetic tilt due to the dipolarization might allow strong KHI even in the later stages of BBF evolution. However, at least 2-D simulations would be needed to examine this possibility in detail.

Nonetheless, our results strongly suggest that the often observed magnetotail flapping and flankward moving waves can be explained by these primary and secondary KHI radiating MHD waves away from the BBF channels.

5. Conclusions

In this paper we have presented a theoretical framework for understanding the role of KHI in the evolution and braking of BBF channels in the magnetotail. We have shown for the first time not only that the earthward BBF channels in the central plasma sheet may become unstable to KHI but perhaps more importantly proposed an explanation for the observed association between BBFs and MHD waves which propagate toward both flanks. According to our model, this can be explained through the excitation and emission of MHD waves from the BBF shear flow boundaries due to the action of the KHI. At sufficiently high flow speeds these KHI waves may extract kinetic energy from the bulk flow in the BBF channel resulting in the braking of the BBFs closer to the Earth. This is shown schematically in Figure 4i.

Future studies could examine the evolution of the KHI sausage and kink modes along BBF channels including the effects of a finite transition thickness layer at the flow channel boundary, perhaps in 2-D including the effects of the changing magnetic field geometry in the BBF as they approach the Earth, which would help to develop a better understanding of the phenomenon across a wider range of wavelengths. Nonlinear studies of the KHI waves along the flow channel boundary could also shed more light especially on the role of the KHI in the evolution and braking of BBFs in the nightside plasma sheet.

Acknowledgments
I.R.M. and R.R. are supported by Discovery grants from Canadian NSERC.

The Editor thanks Martin Volwerk, Katariian Nykyri, and an anonymous reviewer for their assistance evaluating this paper.

References

Angelopoulos, V., W. Baumjohann, C. Kennel, F. Coroniti, M. Kivelson, R. Pellat, R. Walker, H. Lühr, and G. Paschmann (1992), Bursty bulk flows in the inner central plasma sheet, *J. Geophys. Res.*, *97*(A4), 4027–4039.

Angelopoulos, V., et al. (1997), Magnetotail flow bursts: Assosiation to global magnetspheric circulation, relatioship to ionospheric activity and direct evidence for localization, *Geophys. Res. Lett.*, *24*(18), 2271–2274.

Baumjohann, W., G. Paschmann, and H. Lühr (1990), Characteristics of high-speed ion flows in the plasma sheet, *J. Geophys. Res.*, *95*(A4), 3801–3809.

Erkaev, N., V. Semenov, and H. Biernat (2008), Magnetic double gradient mechanism for flapping oscillationsof a current sheet, *Geophys. Res. Lett.*, *35*, L02111, doi:10.1029/2007GL032277.

Forsyth, C., M. Lester, R. Fear, E. Lucek, I. Dandouras, A. Fazakerley, H. Singer, and T. Yeoman (2009), Solar wind and substorm excitation of the wavy current sheet, *Ann. Geophys.*, *27*, 2457–2474.

Golovchanskaya, I., and Y. Maltsev (2005), On the identification of plasma sheet flapping waves observed by cluster, *Geophys. Res. Lett.*, *32*, L02102, doi:10.1029/2004GL021552.

Kozlov, D. A., and A. S. Leonovich (2011), Transformation and absorbtion of MHD oscillations in plane-stratified models of the Earth's magnetosphere, *Geomag. Aeron.*, *51*(8), 1165–1173.

Landau, L. D., and E. M. Lifshitz (1987), *Fluid Mechanics*, pp. 259–262, Pergamon, Oxford, U. K.

Mann, I. R., A. N. Wright, K. J. Mills, and V. M. Nakariakov (1999), Excitation of magnetospheric waveguide modes by magnetosheath flows, *J. Geophys. Res.*, *104*(A1), 333–353.

McPherron, R. L., T.-S. Hsu, J. Kissinger, X. Chu, and V. Angelopoulos (2011), Characteristics of plasma flows at the inner edge of the plasma sheet, *J. Geophys. Res.*, *116*, A00133, doi:10.1029/2010JA015923.

Nakamura, R., et al. (2004), Spatial scale of high-speed flows in the plasma sheet observed by Cluster, *Geophys. Res. Lett.*, *31*, L09804, doi:10.1029/2004GL019558.

Roberts, B. (1991), *MHD Waves in the Sun*, pp. 105–133, Cambridge Univ. Press, Cambridge, U. K.

Sergeev, V., et al. (2003), Current sheet flapping motion and structure observed by Cluster, *Geophys. Res. Lett.*, *30*(6), 1327, doi:10.1029/2002GL016500.

Sergeev, V., A. Runov, W. Baumjohann, R. Nakmura, T. Zhang, A. Balogh, P. Louarnd, J. A. Sauvaud, and H. Rème (2004), Orientation and propagation of current sheet oscillations, *Geophys. Res. Lett.*, *31*, L05807, doi:10.1029/2003GL019346.

Shiokawa, K., W. Baumjohann, and G. Haerendel (1997), Braking of high-speed flows in the near-Earth tail, *Geophys. Res. Lett.*, *24*(10), 1179–1182.

Turkakin, H., R. Rankin, and I. Mann (2013), Primary and secondary compresssible Kelvin-Helmholtz surface waves instabilities on the Earth's magnetopause, *J. Geophys. Res. Space Physics*, *118*, 4161–4175, doi:10.1002/jgra.50394.

Volwerk, M., et al. (2004), Compressional waves in the Earth's neutral sheet, *Ann. Geophys.*, *22*, 303–305.

Volwerk, M., et al. (2005), Plasma flow channels with ULF waves observed by Cluster and Double Star, *Ann. Geophys.*, *23*, 2929–2935.

Volwerk, M., K.-H. Glassmeier, R. Nakamura, T. Takada, W. Baumjohann, B. Klecker, H. Rème, T. Zhang, E. Lucek, and C. Carr (2007), Flow burst-induced Kelvin-Helmholtz waves in the terrestrial magnetotail, *Geophys. Res. Lett.*, *34*, L10102, doi:10.1029/2007GL029459.

Volwerk, M., T. Zhang, K.-H. Glassmeier, A. Runov, W. Baumjohann, A. Balogh, H. Rème, B. Klecker, and C. Carr (2008), Study of waves in the magnetotail region with Cluster and DSP, *Adv. Space Res.*, *41*, 1593–1597, doi:10.1016/j.asr.2007.04.005.